Journal of
Materials Chemistry B

Accepted Manuscript

This article can be cited before page numbers have been issued, to do this please use: N. M. Galdino, G. S. Brehm, R. Bussamara, W. D. G. Gonçalves, G. A. Abarca Anjari and J. D. Scholten, *J. Mater. Chem. B*, 2017, DOI: 10.1039/C7TB02582C.

ROYAL SOCIETY OF CHEMISTRY

rsc.li/materials-b

Table of Contents

View Article Online
DOI: 10.1039/C7TB02582C

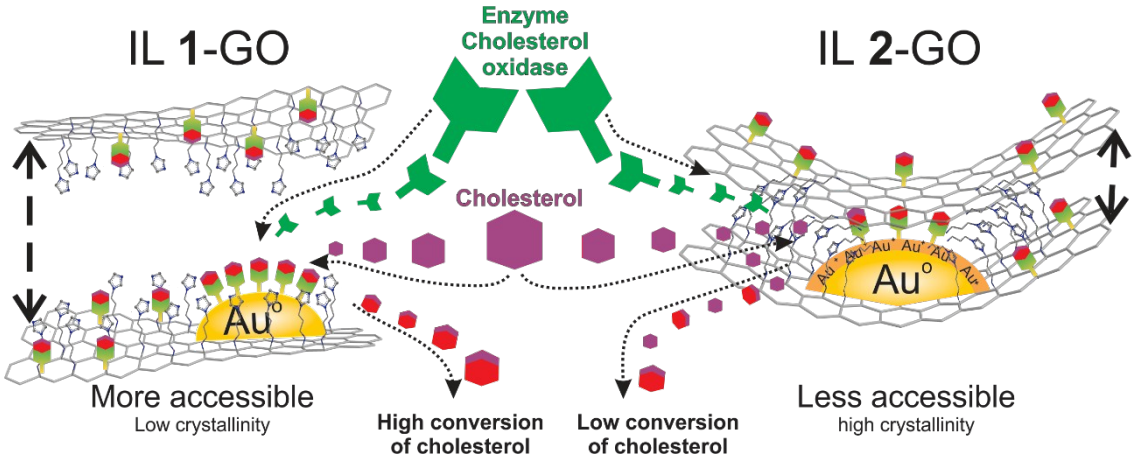

The sputtering deposition of Au nanoparticles onto ionic liquid-graphene oxide combined with cholesterol oxidase affords an efficient biosensor for cholesterol detection.

View Article Online
DOI: 10.1039/C7TB02582C

Journal Name

COMMUNICATION

Sputtering deposition of gold nanoparticles onto graphene oxide functionalized with ionic liquids: biosensor materials for cholesterol detection

Received 00th January 20xx,
Accepted 00th January 20xx

DOI: 10.1039/x0xx00000x

www.rsc.org/

Nathália M. Galdino, Gabriele S. Brehm, Roberta Bussamara,* Wellington D. G. Gonçalves, Gabriel Abarca and Jackson D. Scholten*

Ionic liquid (IL)-functionalized graphene oxide (GO) containing gold nanoparticles (Au NPs) (5.4-5.9 nm) deposited by sputtering combined with cholesterol oxidase appears to be a suitable and efficient biosensor for total cholesterol detection. These biosensors showed good linear range (25-470 µmol/L) for total cholesterol determination by colorimetric tests. In addition, control experiments in the presence of interferents demonstrated that the hybrid materials provided a selective detection of total cholesterol. The biosensing activities obtained for the hybrid materials indicate that these compounds are potential biosensors for clinical applications.

Nowadays, non-transmissible chronic diseases are a worldwide problem and a threat to health and human development. In particular, one of the risk factors for the development of cardiovascular disease, diabetes, atherosclerosis and hypertension is a high level of cholesterol.[1, 2] On the other hand, low level of cholesterol in blood may be associated with depression, cancer and cerebral hemorrhage.[3] Cholesterol is a long-chain polycyclic alcohol, which is transported in the blood plasma of animals. Also, it is an essential component for the cell membrane and a precursor for the synthesis of other biological materials.[4] Rapid and accurate determination of cholesterol level is fundamental to prevent diseases as mentioned above. The colorimetric method has been used for cholesterol sensing because it is easy to apply, more economical when compared to electrochemical tests, uses simple instrumentation and makes naked eye detection possible without requiring additional measurements.[5] In this context, biosensors present many advantages compared to classical methods: low cost, rapid detection, high selectivity and sensitivity, and the possibility to produce portable devices for home or *in situ* detection.[2] The development of new materials that allow efficient enzyme immobilization to maintain high activity and stability during the process is of fundamental importance in order to build a high performance biosensor for portable measurements with the same accuracy as clinical analysis. For this purpose, several kinds of hybrid biosensors have been prepared and tested, such as Au/cysteamine/Au NPs/ChOx electrode (ChOx = cholesterol oxidase),[6] Pt/LDHs-chitosan/ChOx electrode (LDHs = layered double hydroxides),[7] L-cysteine-rGO/GCE/Au NPs/ChOx (rGO = reduced graphene oxide, GCE = glassy carbon electrode),[8] Au@Ag core-shell NPs,[5] ChOx/$NiFe_2O_4$/CuO/FeO-chitosan/ITO (ITO: indium-tin-oxide glass substrate),[9] ChOx-ChEt/GPTMS/ITO (GPTMS: (3-glycidoxypropyl)trimethoxysilane),[10] ChOx-ChEt/$NiFe_2O_4$ NPs-chitosan/ITO,[11] ChOx-ChEt/Cu_2O NPs-chitosan/ITO[12] and ChOx-ChEt/Tm_2O_3 nanorods/ITO.[13] More examples of biosensors for cholesterol determination can be found in a previous review.[2] Ionic liquids (ILs) have been used as alternative materials in biosensing applications.[14, 15] Moreover, these ionic compounds have also been employed as modifiers in hybrid supports[16-19] applied as cholesterol biosensors. However, to the best of our knowledge, there are no examples of the use of a sputtering technique to generate small and clean Au NPs on IL-modified supports and their application in the detection of cholesterol. In fact, the most common procedure to prepare Au NPs is from the reduction of gold metal precursors, which generates undesired by-products and remaining ligands. These undesired compounds can coordinate to the metal surface and decrease the particle's activity. Motivated by the advantages of ILs[20] and GO,[21] in this work we combined these compounds and sputtered Au NPs to produce a simple and efficient material to be used as a biosensor for colorimetric determination of total cholesterol. In fact, the synergistic effect of the IL fragments covalently attached to the GO (rGO) together with the presence of small and clean Au NPs provides a suitable hybrid material.

Instituto de Química, UFRGS, Av. Bento Gonçalves 9500, Agronomia, CEP 91501-970, Porto Alegre-RS, Brazil.

E-mail: roberta.bussamara@ufrgs.br

E-mail: jackson.scholten@ufrgs.br; Tel: +55 51 3308 9633.

† Electronic Supplementary Information (ESI) available: Experimental section and additional figures. See DOI: 10.1039/x0xx00000x

View Article Online
DOI: 10.1039/C7TB02582C

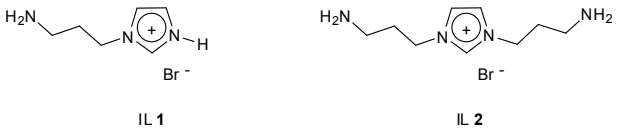

Fig. 1 Amine-functionalized ILs used as modifiers in the GO supports.

The preparation of the amine-functionalized ILs (Fig. 1) and the GO modified with ILs was performed according to the methods described in Supporting Information (SI). The functionalized GO supports were characterized by FTIR, Raman, X-ray diffraction (XRD) and X-ray photoelectron spectroscopy (XPS) (see SI). By Raman analyses of the IL-GO supports (Fig. S2), it was possible to evaluate the disorder and defects using the signals D and G – sp^2 carbon vibrations – localized at 1360 cm^{-1} and 1560 cm^{-1}, respectively.[22, 23] The harmonic signal 2D (2680 cm^{-1}) is related to the number of graphene sheets[24] while the signal D+D' is due to defects in the carbon structure.[23] Comparing the oxide precursors (GO) before functionalization, only luminescence could be observed, which is characteristics of GO.[25] Concerning to evaluate the defects, we considered the relation between the intensity of signals D and G (I_D/I_G); a higher value was obtained for IL **1**-GO, indicating the presence of more structural defects, decreasing the sp^2 sites in the matrix and consequently the graphitic sites. In both cases, IL **1**-GO and IL **2**-GO, the signals D and D+D' were significant, which indicates the presence of defects and low sp^2 conjugation of graphene sites. The size of the graphitic sites was estimated by using the Tuinstra and Koenig relation,[23] achieving 7.43 and 8.60 for IL **1**-GO and IL **2**-GO, respectively (for more details, see SI). The minor graphitic size observed for the sample IL **1**-GO suggests that functionalization with IL **1** provides a minor interaction among the carbon sheets. In other words, IL **1**-GO adopts a less organized structure of graphene sheets while for IL **2**-GO the IL may act as a spacer among them, providing a graphite-like structure. The Au NPs were deposited onto the IL-functionalized GO support by a sputtering technique (Fig. 2). This deposition method was chosen because it is a facile and clean procedure to generate well-distributed nanoscale particles.[26]

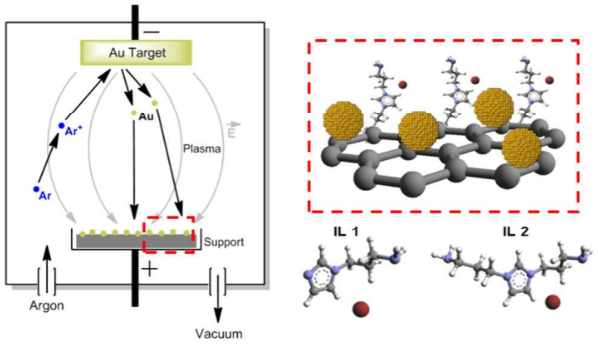

Fig. 2 Sputtering deposition of Au NPs onto the IL-functionalized GO supports.

The supported Au NPs were analyzed by TEM, XRD and XPS analysis. TEM measurements evidenced the formation of Au NPs with 5.4 ± 2.0 nm on IL **1**-GO and 5.9 ± 2.1 nm on IL **2**-GO (Fig. 3). Moreover, it was observed well-dispersed particles with a spherical-like shape deposited on the IL-GO sheets, although few large particles could also be detected. The controlled size distribution for both samples is a significant advantage of the sputtering method, because in this case it was possible to control the experimental parameters such as current, voltage and deposition time in order to obtain particles with a similar average size. It is expected that the IL groups attached onto the GO provide additional stabilization for the supported Au NPs, similar to that observed in other metal NPs immobilized in IL-functionalized supports.[27, 28]

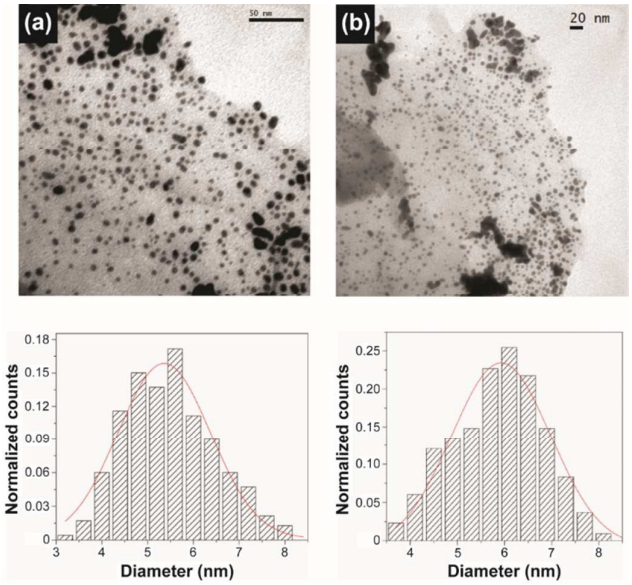

Fig. 3 TEM micrographs of the Au NPs supported on (a) IL **1**-GO and (b) IL **2**-GO with their respective size distribution histograms.

XRD measurements confirmed the presence of Au NPs on the supports showing crystalline particles with *fcc* structure, where Au NPs presented their two characteristic peaks at 38.2° (111) and 40.5° (200), respectively (Fig. S3). After the oxidation of graphite by the Hummers method, the XRD pattern of GO showed a sharp diffraction peak at 2Θ = 9.5° (d-spacing = 0.93 nm) due to the intercalation of functional groups containing oxygen between the layers of graphite. Subsequently, the functionalization of GO (IL **1**-GO and IL **2**-GO) showed a shift at 2Θ = 7.5° (d-spacing = 1.18 nm) and 2Θ = 7.3° (d-spacing = 1.21 nm), respectively, which indicates the intercalation of the ILs among the graphene layers. The peak at 2Θ = 28.3° (d-spacing = 0.315 nm) provides similar spacing to a graphite structure, which indicates that the graphene oxide sample functionalized with IL **2** adopted a partially crystalline system, which can be related to simultaneous interaction of the amine groups of the imidazolium cation with the carbon sheets. It is reasonable to suppose that the IL cation acts as a bridge crosslinking the two carbon sheets, modifying the interplanar spacing of the GO. It is noteworthy that this 28.3° signal was not observed for IL **1**-GO, which suggests a preferred graphene-like arrangement in this case.

View Article Online
DOI: 10.1039/C7TB02582C

In order to evaluate and compare the surface chemical composition of the GO, IL-GO and Au NPs/IL-GO samples, XPS analyses were performed. XPS peaks for O 1s, N 1s, C 1s and Au 4f core-level regions were observed. In Fig. 4 is shown the typical XPS spectra of the C 1s region of graphite and GO. High-resolution C 1s spectra were decomposed into five peaks, corresponding to C-C, C=C, C-O-C, C=O and O=C-O, which were in agreement with the literature[29, 30] and confirm significant structural changes during the oxidation process from graphite to GO. Indeed, the C/O atomic ratio decreased from 24.13 for graphite to 3.84 for GO,[31] in accordance with FTIR spectra (see Fig. S1). After reduction and functionalization with IL, the peak intensities of oxide moieties decreased, accompanied by an increase of the sp^2 carbon peak, which indicates the presence of cationic IL fragments attached to the carbon network. The N 1s peak region showed signals associated to the imidazolium ring,[32] a shoulder at 398.9 eV confirms the presence of NH and a peak at 405.2 eV confirms the presence of NH_2.[30, 33] The IL-GO supports containing Au NPs deposited by sputtering were also analyzed (Fig. 4). The Au $4f_{7/2}$ photoelectron peak appeared at 83.87 eV (SI) and peak doublet separation was consistent with the Au^0 state (3.7 eV).[34] The relative Au content in the samples was estimated to be around 4% by XPS. Although only metallic Au was found in the Au NPs/IL **1**-GO sample, for Au NPs/IL **2**-GO, Au^0 and $Au^{\delta+}$ components were observed. The presence of $Au^{\delta+}$ component may have an effect on the biosensing activity of the Au NPs/IL **2**-GO material.

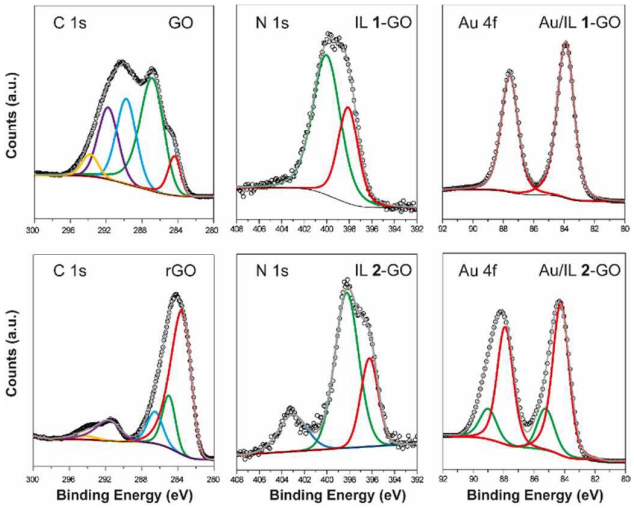

Fig. 4 XPS measurements in the C 1s, N 1s and Au 4f regions of the IL-GO supports and the Au NPs/IL-GO materials. Black points represent the experimental data and the gray line represents the best fitting. In the C 1s region: red, green, light blue, purple and yellow solid lines represent C=C, C-C C-O-C, C=O and O=C-O chemical components, respectively. The C 1s region of the rGO represents typical behavior after functionalization of GO samples (IL-modified GO). In the N 1s region: red, green and light blue solid lines represent NH (anchored to graphene), N (imidazolium ring) and NH_2 chemical components, respectively. In the Au 4f region: red and green solid lines represent Au^0 and $Au^{\delta+}$ chemical components, respectively.

For biosensor construction, the ChOx enzyme was immobilized on the hybrid materials Au NPs/IL **1**-GO and Au NPs/IL **2**-GO and tested for total cholesterol detection by colorimetric assay. Biosensor responses were measured using standard cholesterol solutions at body temperature (see details in SI). Fig. 5 shows the plot of enzyme response vs. cholesterol concentration. Both free enzyme (free-ChOx), ChOx-Au NPs/IL **1**-GO and ChOx-Au NPs/IL **2**-GO biosensors showed linear cholesterol detection at concentrations between 10 and 95 mg/L with correlation coefficients of 0.9991, 0.9951 and 0.9890, respectively. The sensitivity values were determined as 0.0127 L/mg and 0.0097 L/mg for ChOx-Au NPs/IL **1**-GO and ChOx-Au NPs/IL **2**-GO, respectively. These results reveal that both materials developed in this work allowed efficient action of the enzyme in the reaction medium, showing high potential for application as biosensors. Even though the percentage of ChOx immobilized in both materials was similar (93% for ChOx-Au NPs/IL **1**-GO and 92% for ChOx-Au NPs/IL **2**-GO), the biosensor ChOx-Au NPs/IL **1**-GO showed a greater response to cholesterol compared to the ChOx-Au NPs/IL **2**-GO biosensor (Fig. 5). In Fig. 5 (b and c) it is observable by naked eye the red color gradient due to the increase of cholesterol concentration in the samples.

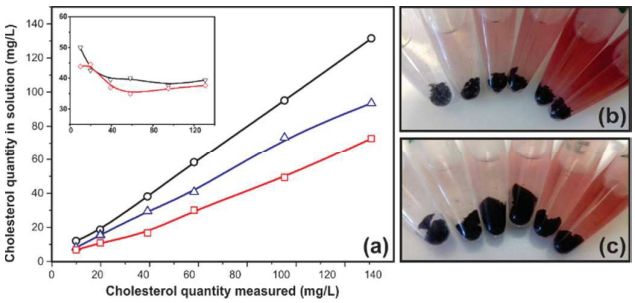

Fig. 5 (a) Detection of cholesterol at different concentrations: (○) free-ChOx, (△) ChOx-Au NPs/IL **1**-GO, (□) ChOx-Au NPs/IL **2**-GO; inset: (▽) ChOx-GO and (◊) ChOx-Au NPs/GO. Typical colorimetric tests using (b) ChOx-Au NPs/IL **1**-GO and (c) ChOx-Au NPs/IL **2**-GO.

Regarding to evaluate the biosensor response, the recovered activity (activity percentage of the enzyme in the material relative to the free enzyme) was calculated. Compared with free-ChOx, the ChOx-Au NPs/IL **1**-GO and ChOx-Au NPs/IL **2**-GO biosensors retained a maximum of 76% and 54% of ChOx activity, respectively. The higher recovered activity for the ChOx-Au NPs/IL **1**-GO biosensor is probably due to the graphene-like structure of this material, which possibly provides more availability and better diffusion of cholesterol to the enzyme active site. It is also possible that the graphite-like structure of the ChOx-Au NPs/IL **2**-GO biosensor results in less exposure of the enzyme's active sites, decreasing the activity. Moreover, the presence of $Au^{\delta+}$ may facilitate the coordination of additional electron-donating groups to the surface of the Au NP, which possibly interfere in the biosensing behavior of this material compared to Au NPs/IL **1**-GO. As another important aspect, the isoelectric point of the cholesterol oxidase is 5.4, indicating that the enzyme has a negative charge in the working pH (7.0). This allows the enzyme to bind to a positively charged matrix

View Article Online
DOI: 10.1039/C7TB02582C

as the Au NP's surface. Then, it is expected that the enzyme will interact more strongly with the Au NPs in the IL **2**-GO material due to the presence of surface $Au^{\delta+}$ species observed by XPS.

Table 1 Comparison of the analytical response in cholesterol detection of various biosensors

Entry	Material	Determination method	Linear range (µmol/L)	Reference
1	ChOx-Au NPs/IL **1**-GO	Colorimetric	25-470	Present work
2	ChOx-Au NPs/IL **2**-GO	Colorimetric	25-470	Present work
3	ChOx/Au@Ag core-shell NPs	Colorimetric	0.3-300	[5]
4	ChOx-IL-capped Au NPs/GCE	Voltametric	0.1-50	[35]
5	ChOx/catalase/rGO-IL/GCE	Chronoamperometric	0.25-5/5-215[a]	[18]
6	ChOx-ChEt[b]/Pt NPs/graphene-nafion/GCE	Amperometric	5-35	[36]

[a]Two range for the same material; [b]ChEt = cholesterol esterase.

In addition, the biosensor's stability was tested. The response of both materials to cholesterol was analyzed after 24 and 115 h. At 115 h, cholesterol detection decreased to 52% and 81% of the initial value for ChOx-Au NPs/IL **1**-GO and ChOx-Au NPs/IL **2**-GO biosensors, respectively, probably due to enzyme desorption of the material or a decrease of ChOx activity. Therefore, the hybrid materials showed good stability under the tested conditions, indicating that these biosensors can be used in clinical analyses. The superior stability of the ChOx-Au NPs/IL **2**-GO biosensor may be associated with a possible stronger interaction between the enzyme and the Au NPs in this material. To improve the knowledge about the IL role in biosensor efficiency, the enzyme was immobilized only on graphene oxide (ChOx-GO) and on graphene oxide containing gold nanoparticles (ChOx-Au NPs/GO). Besides the percentage of ChOx immobilized on both materials (73% for ChOx-GO and ChOx-Au NPs/GO) being slightly less than for ChOx-Au NPs/IL **1**-GO and ChOx-Au NPs/IL **2**-GO materials, the response of ChOx-GO and ChOx-Au NPs/GO biosensors to cholesterol detection was not linear (Fig. 5). These results evidence that the presence of IL in biosensor materials has a positive synergistic effect, which is important to distinguish the variation of cholesterol quantities. In addition, it is important to note that in the cases where non-functionalized GO (without IL) was employed, the ChOx recovered activity was superior to the free ChOx (see Table S1). These observations cannot be related to the enzyme activity on the cholesterol, but due to the oxidizing agents present at the GO surface that may react with the color reagent. Considering all the results obtained in this work, Scheme 1 provides a schematic proposal for the interaction of the cholesterol molecule with the functionalized hybrid materials.

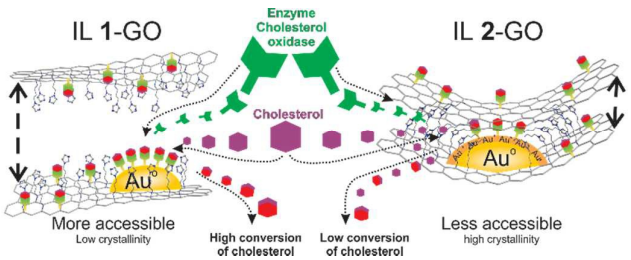

Scheme 1 Proposed interaction of cholesterol with the ChOx-Au NPs/IL-GO materials.

Notably, the materials produced in this work showed a cholesterol detection range from 25 to 470 µmol/L, which is a large range compared to similar state-of-the-art graphene-based materials found in the literature (Table 1). This large linear range demonstrates that the present materials can be used to detect low (<150 µmol/L),[3] medium and high (>260 µmol/L)[1] levels of cholesterol, considering an analogous test performed in clinical analysis (with a plasma dilution factor of 1:20).[37] As control experiments, the hybrid materials were tested in the presence of common interferents such as glucose, ascorbic acid and uric acid in order to verify a possible interference effect in the biosensing activities. The results indicate that the detection of the interferents is negligible and the hybrid materials were selective towards total cholesterol (Fig. S7). Besides the large detection range, a considerable advantage of these hybrid materials is the high enzyme recovered activity, sensitivity and selectivity for total cholesterol that allow the application of a typical clinical method and further reuse the material. The robustness and efficiency of these hybrid materials at high cholesterol concentration can be associated to the synergistic effect of IL-functionalized GO and the small/clean Au NPs obtained by the sputtering technique. Therefore, the combination of IL-GO and Au NPs produced by the sputtering method generated biosensors with a large detection range that will be able to extend the cholesterol quantification using other methodologies.

Conclusions

In summary, the sputtering deposition of Au NPs onto GO modified with amine-functionalized ILs generates promising hybrid materials to be used as efficient biosensors for cholesterol detection. This physical method employed to generate NPs has the advantage of producing small, clean and controlled size particles, which are difficult to obtain by using the classical chemical reduction of metal precursors. The ChOx

View Article Online
DOI: 10.1039/C7TB02582C

was efficiently immobilized on Au NPs/IL **1**-GO and Au NPs/IL **2**-GO materials and showed a good recovered activity on both supports. Preliminary experiments applying these hybrid materials as cholesterol biosensors showed satisfactory results to identify individuals with low to high cholesterol levels using a practical naked eye colorimetric test. Indeed, the target biomolecule was detected with excellent efficiency and linearity. Moreover, the presence of IL in the material composition allows a synergistic effect with the enzyme that is essential for the linear detection of cholesterol. Therefore, the combination of Au NPs and IL-GO produces robust and selective biosensors with large detection range for total cholesterol, opening new possibilities for the design of active materials to detect biochemical target compounds in clinical applications.

Conflicts of interest

There are no conflicts of interest to declare.

Acknowledgements

The authors thank the Brazilian agencies CNPq, CAPES and FAPERGS for financial support and LNLS (Campinas-SP) for the XPS analysis.

References

1. S. Mann, C. Beedie and A. Jimenez, *Sports Med.*, 2014, **44**, 211-221.
2. S. K. Arya, M. Datta and B. D. Malhotra, *Biosens. Bioelectron.*, 2008, **23**, 1083-1100.
3. M. A. Crook, U. Velauthar, L. Moran and W. Griffiths, *Ann. Clin. Biochem.*, 1999, **36**, 613-616.
4. J. Hu, Z. H. Zhang, W. J. Shen and S. Azhar, *Nutr. Metab.*, 2010, **7**, 47.
5. X. H. Zhang, M. Wei, B. J. Lv, Y. J. Liu, X. Liu and W. Wei, *RSC Adv.*, 2016, **6**, 35001-35007.
6. N. Zhou, J. Wang, T. Chen, Z. G. Yu and G. X. Li, *Anal. Chem.*, 2006, **78**, 5227-5230.
7. S. N. Ding, D. Shan, T. Zhang and Y. Z. Dou, *J. Eletroanal. Chem.*, 2011, **659**, 1-5.
8. M. Zhang, R. Yuan, Y. Chai, S. Chen, H. Zhong, C. Wang and Y. Cheng, *Biosens. Bioelectron.*, 2012, **32**, 288-292.
9. J. Singh, M. Srivastava, P. Kalita and B. D. Malhotra, *Process Biochem.*, 2012, **47**, 2189-2198.
10. S. Kumar, J. Singh, V. V. Agrawal, M. Ahamad and B. D. Malhotra, *Anal. Methods*, 2011, **3**, 2237-2245.
11. J. Singh, A. Roychoudhury, M. Srivastava, V. Chaudhary, R. Prasanna, D. W. Lee, S. H. Lee and B. D. Malhotra, *J. Phys. Chem. C*, 2013, **117**, 8491-8502.
12. J. Singh, M. Srivastava, A. Roychoudhury, D. W. Lee, S. H. Lee and B. D. Malhotra, *J. Phys. Chem. B*, 2013, **117**, 141-152.
13. J. Singh, A. Roychoudhury, M. Srivastava, P. R. Solanki, D. W. Lee, S. H. Lee and B. D. Malhotra, *Nanoscale*, 2014, **6**, 1195-1208.
14. M. Ratel, A. Provencher-Girard, S. S. Zhao, J. Breault-Turcot, J. Labrecque-Carbonneau, M. Branca, J. N. Pelletier, A. R. Schmitzer and J. F. Masson, *Anal. Chem.*, 2013, **85**, 5770-5777.
15. D. T. Wu, P. F. Cai, Z. H. Tao and Y. J. Pan, *Anal. Chim. Acta*, 2016, **902**, 174-181.
16. A. I. Gopalan, K. P. Lee and D. Ragupathy, *Biosens. Bioelectron.*, 2009, **24**, 2211-2217.
17. A. Safavi and F. Farjami, *Biosens. Bioelectron.*, 2011, **26**, 2547-2552.
18. M. B. Gholivand and M. Khodadadian, *Biosens. Bioelectron.*, 2014, **53**, 472-478.
19. S. Y. Wu, Y. X. Wang, H. Mao, C. Wang, L. X. Xia, Y. Zhang, H. Ge and X. M. Song, *RSC Adv.*, 2016, **6**, 59487-59496.
20. J. Dupont, *Acc. Chem. Res.*, 2011, **44**, 1223-1231.
21. D. R. Dreyer, S. Park, C. W. Bielawski and R. S. Ruoff, *Chem. Soc. Rev.*, 2010, **39**, 228-240.
22. A. Eckmann, A. Felten, A. Mishchenko, L. Britnell, R. Krupke, K. S. Novoselov and C. Casiraghi, *Nano Lett.*, 2012, **12**, 3925-3930.
23. L. G. Cançado, A. Jorio, E. H. M. Ferreira, F. Stavale, C. A. Achete, R. B. Capaz, M. V. O. Moutinho, A. Lombardo, T. S. Kulmala and A. C. Ferrari, *Nano Lett.*, 2011, **11**, 3190-3196.
24. A. Gupta, G. Chen, P. Joshi, S. Tadigadapa and P. C. Eklund, *Nano Lett.*, 2006, **6**, 2667-2673.
25. S. Hermanova, M. Zarevucka, D. Bousa, M. Pumera and Z. Sofer, *Nanoscale*, 2015, **7**, 5852-5858.
26. K. I. Okazaki, T. Kiyama, K. Hirahara, N. Tanaka, S. Kuwabata and T. Torimoto, *Chem. Commun.*, 2008, 691-693.
27. L. Luza, A. Gual, D. Eberhardt, S. R. Teixeira, S. S. X. Chiaro and J. Dupont, *ChemCatChem*, 2013, **5**, 2471-2478.
28. L. Foppa, L. Luza, A. Gual, D. E. Weibel, D. Eberhardt, S. R. Teixeira and J. Dupont, *Dalton Trans.*, 2015, **44**, 2827-2834.
29. C. K. Chua, Z. Sofer and M. Pumera, *Angew. Chem. Int. Ed.*, 2016, **55**, 10751-10754.
30. H. F. Yang, C. S. Shan, F. H. Li, D. X. Han, Q. X. Zhang and L. Niu, *Chem. Commun.*, 2009, 3880-3882.
31. S. Shamaila, A. K. L. Sajjad and A. Iqbal, *Chem. Eng. J.*, 2016, **294**, 458-477.
32. K. R. J. Lovelock, I. J. Villar-Garcia, F. Maier, H. P. Steinruck and P. Licence, *Chem. Rev.*, 2010, **110**, 5158-5190.
33. Z. J. Wang, Q. X. Zhang, D. Kuehner, X. Y. Xu, A. Ivaska and L. Niu, *Carbon*, 2008, **46**, 1687-1692.
34. A. Y. Klyushin, M. T. Greiner, X. Huang, T. Lunkenbein, X. Li, O. Timpe, M. Friedrich, M. Havecker, A. Knop-Gericke and R. Schlogl, *ACS Catal.*, 2016, **6**, 3372-3380.
35. M. J. Dong, Z. H. Nan, P. P. Liu, Y. J. Zhang, Z. H. Xue, X. Q. Lu and X. H. Liu, *Electrochim. Acta*, 2014, **132**, 465-471.
36. R. S. Dey and C. R. Raj, *J. Phys. Chem. C*, 2010, **114**, 21427-21433.
37. C. C. Allain, L. S. Poon, C. S. G. Chan, W. Richmond and P. C. Fu, *Clin. Chem.*, 1974, **20**, 470-475.